Applied Science and Engineering Progress, Vol. 13, No. 4, pp. 336–345, 2020

Research Article

Stress Intensity Factor K_I and Crack–hard Inclusion Interaction Study of a Single Edge Cracked Plate by Adaptive Remeshing and Photoelasticity

Wiroj Limtrakarn*
Department of Mechanical Engineering, Faculty of Engineering, Thammasat University, Rangsit Campus, Pathum Thani, Thailand

* Corresponding author. E-mail: limwiroj@engr.tu.ac.th DOI: 10.14416/j.asep.2019.02.006
Received: 23 July 2018; Revised: 15 October 2018; Accepted: 21 November 2018; Published online: 18 February 2019

Abstract
An adaptive remeshing and photoelasticity techniques are presented to determine the stress intensity factors K_I and crack-hard inclusion interaction of a single edge cracked plate for two-dimensional fracture mechanics problems. The paper starts from describing two-dimensional linear fracture mechanics theory and an adaptive remeshing *H* method using the quadrilateral and triangular elements. The computational procedure and related finite element equations are explained. The photoelastic theory and its experimental procedure with the use of the stress optic laws are then described. The photoelasticity prototype is designed and built. Performance of adaptive remeshing method is evaluated by analyzing a single edge cracked plate made from polycarbonate. A crack plate with a hard inclusion is then studied for stress intensity factor and crack-hard inclusion interaction. The hard inclusion is made from aluminum. The K_I stress intensity factor is found to be a function of the crack length per width. The results of adaptive remeshning method and the photoelasticity technique are compared with Brown's study. This example demonstrates the efficiency of the adaptive remeshing method to provide accurate solutions as compared to those from the photoelastic technique. Then, crack-hard inclusion interaction is studied by varying stress intensity ratio and *E* ratio. The crack-hard inclusion interaction behavior is formulated in exponential equation, i.e. cracking tip shielding function. The cracking tip shielding function shows that maximum stress intensity ratio reduces rapidly if *E* ratio increases. The normalized stress intensity factor is as a convergence exponential function of *E* ratio.

Keywords: Stress intensity factor, Crack-hard inclusion interaction, Adaptive remeshing, Photoelasticity

1 Introduction

Nowadays composite materials are widely used to make a part or all in many products and machine. The popular usage is from the benefit of light weight, low product cost and easy to build. Nonhomogeneous material is one physical property of composite material. An arbitrary strength or failure is still occurred and should be studied how to control or predict. Life prediction under crack propagation is interested to define the arrangement of composite composition. Young modulus ratio of inclusion and plate is influence to crack tip characteristics. Propagation of crack can be predicted by the stress intensity factors K_I near crack tip on composite material. Several numerical methods and nondestructive experimental techniques (NDT) are currently used to determine phenomena of crack propagation. Photoelasticity technique is one of NDT has been employed to determine the stress intensity factors and inclusion effect [1]–[6]. Its principle is based on the optic–experimental interference by analyzing the maximum shear stress induced in the transparent

Please cite this article as: W. Limtrakarn, "Stress intensity factor K_I and crack–hard inclusion interaction study of a single edge cracked plate by adaptive remeshing and photoelasticity," *Applied Science and Engineering Progress*, vol. 13, no. 4, pp. 336–345, Oct.–Dec. 2020.

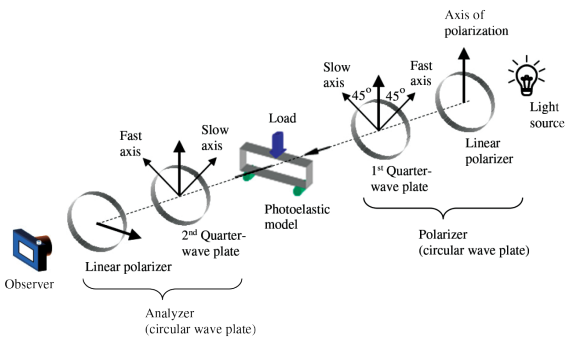

Figure 1: Photoelastic model under loading.

or birefringent of the photoelastic model under loading and crack tip configuration. The phenomenon is observed by looking through the optical elements, i.e., the polarizer and analyzer of the polariscope as shown in Figure 1. The results provide information that can be applied directly to metal prototypes by using the law of similarity. At present, the stress intensity factor and crack propagation characteristics are studied in several numerical methods, i.e. the finite element method [7]–[10], the meshless method [11], [12], the manifold method with virtual crack extension [13], and the boundary element method [14], [15]. Some researchers have evaluated crack-inclusion interactions and crack tip shielding by photoelasticity technique [16]–[19] and other experiments [20]–[23].

In this paper, theory of two-dimensional linear elastic fracture mechanics is first described. The adaptive finite element method with 8-node quadrilateral elements near the crack tip is explained. Photoelasticity technique is then described. The stress intensity factors K_I varied with crack length ratios (a/W), between 0.2 and 0.6, on single edge cracked plate is used to compare results of photoelasticity technique, adaptive finite element method, and Brown [24]. Next, inclusion effect is investigated. Hard inclusion with cylinder diameter 3.6 millimeters on single edge cracked plate is selected to study the phenomena of stress intensity factor K_I by vary crack length ratios (0.2 to 0.6) and constant modulus of elasticity ratio ($E_{inclusion}/E_{plate}$, E_r = 28) using adaptive finite element method and photoelasticity technique. An adaptive finite element method is then used to predict stress intensity factors K_I and crack tip shielding on single edge cracked plate varied crack length ratios (0.2 to 0.6) and young modulus ratios (1.1 to 50). Finally, cracking tip shielding function depending on young modulus ratio and crack length ratios is estimated.

2 Theory

2.1 *Stress and stress intensity factor equation*

The stress and stress intensity factors relationship in mode I and II based on 2D linear elastic fracture mechanics theory [25], neglect non-singular and higher-order terms, is expressed as,

$$\sigma_x = \frac{1}{\sqrt{2\pi r}}\left[K_I \cos\frac{\theta}{2}\left(1-\sin\frac{\theta}{2}\sin\frac{3\theta}{2}\right) - K_{II}\sin\frac{\theta}{2}\right]\left(2-\cos\frac{\theta}{2}\cos\frac{3\theta}{2}\right) \quad (1)$$

$$\sigma_y = \frac{1}{\sqrt{2\pi r}}\left[K_I \cos\frac{\theta}{2}\left(1-\sin\frac{\theta}{2}\sin\frac{3\theta}{2}\right) + K_{II}\sin\frac{\theta}{2}\cos\frac{\theta}{2}\cos\frac{3\theta}{2}\right] \quad (2)$$

$$\tau_{xy} = \frac{1}{\sqrt{2\pi r}}\left[K_I \sin\frac{\theta}{2}\cos\frac{\theta}{2}\cos\frac{3\theta}{2} + K_{II}\cos\frac{\theta}{2}\left(1-\sin\frac{\theta}{2}\sin\frac{3\theta}{2}\right)\right] \quad (3)$$

where K_I and K_{II} are the stress intensity factors for mode I (opening mode) and mode II (tearing mode); r and θ are the distance and the angle in the polar coordinates as shown in Figure 2; σ_x and σ_y are the normal stresses in x and y directions, respectively, and τ_{xy} is the shearing stress.

The stress intensity factor at the crack tip (K) is explained by [26] [Equation (4)],

$$K = F\sigma_\infty\sqrt{\pi a} \quad (4)$$

where F is the geometry factor that depends on the dimensions of problem, σ_∞ is the far-field stress and a is the crack length.

By displacement extrapolation the stress intensity factors K_I and K_{II} can be determined near the crack tip.

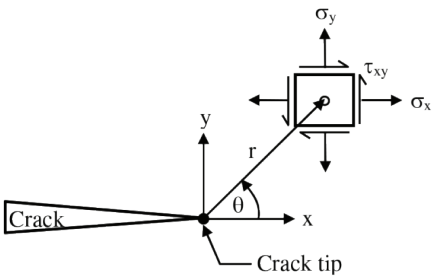

Figure 2: State of stresses in polar coordinates from crack tip.

These stress intensity factors are formulated in,

$$K_I = \frac{E}{3(1+\nu)(1+\kappa)}\sqrt{\frac{2\pi}{L}}\left(4(v_b - v_d) - \left(\frac{v_c - v_e}{2}\right)\right) \quad (5)$$

$$K_{II} = \frac{E}{3(1+\nu)(1+\kappa)}\sqrt{\frac{2\pi}{L}}\left(4(u_b - u_d) - \left(\frac{u_c - u_e}{2}\right)\right) \quad (6)$$

where E is young modulus, ν is the Poisson's ratio, L is the element length, u and v are the displacement components in x- and y-directions, respectively, as well as κ is the elastic parameter and equals 3–4ν for plane strain problem and (3 – ν)/(1 + ν) for plane stress problem. The subscripts of u and v represent their positions for the nodes of the elements near the crack tip as depicted in Figure 3(a). Figure 3(b) provides detail of the 8-node quadrilateral element with their mid-side node positions, while nodes 1, 4, and 8 are collapsed and placed together at the crack tip.

2.2 *Finite element formulation*

The finite element equations can be derived from the 2D governing differential equations of equilibriums. The derived finite element equations are written in matrix form as [Equation (7)],

$$[K]\ \{u\} = \{F\} \quad (7)$$

where $[K]$ is the element stiffness matrix [27], $\{u\}$ is the vector of the element nodal displacements and $\{F\}$ is the element load vector.

Due to improve accuracy near crack tip the high-order element interpolation functions is preferred. The eight–node quadrilateral elements (Q8) are selected to build a circular zone around the crack tip. Q8 element has mid–side nodes displaced from its nominal position to quarter points of the tip as shown in Figure 3(a). The radius of the circular zone is defined no longer than one–eight of the initial crack length, with roughly one element every 30° in the circumferential direction [28]. The four–node quadrilateral elements (Q4) are selected to connect the Q8 elements and construct the triangular elements (T3) in domain far from the crack tip as shown in Figure 4. K_I and K_{II} can be computed by substitute nodal displacement in Equations (5) and (6), respectively.

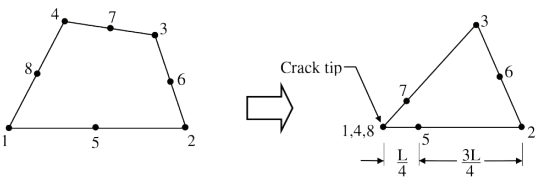

(a) A quarter–point eight–node quadrilateral element.

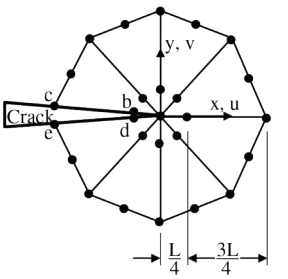

(b) Quarter–point quadrilateral elements around crack tip

Figure 3: Eight-node quadrilateral element around crack tip.

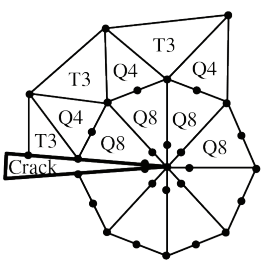

Figure 4: Combination of three element types surrounding crack tip.

2.3 *Adaptive remeshing technique*

H method is implemented as the adaptive remeshing techniques in this paper. The initial finite element model

is first construct. Then, elements in the initial mesh is refined into smaller elements or larger elements [29]–[31]. The adaptive mesh technique generates an entirely new mesh based on the solution obtained from an earlier result on mesh [32], [33]. The core concept is to build a new mesh that consists of small elements in the high solution gradients domains and large elements in the other domains where low solution gradients appear. An appropriate element sizes at different locations in the domain is determined. The von Mises stress σ gradients is used as element size factor. The second derivatives of the von Mises stress at a point with respect to global coordinates x and y are required. Based on the principal directions concept from a given state of stresses at a point, the principal quantities in the principal directions X and Y where the cross-derivatives vanish are determined [Equation (8)]:

$$\begin{bmatrix} \frac{\partial^2\sigma}{\partial x^2} & \frac{\partial^2\sigma}{\partial x\partial y} \\ \frac{\partial^2\sigma}{\partial x\partial y} & \frac{\partial^2\sigma}{\partial y^2} \end{bmatrix} \Rightarrow \begin{bmatrix} \frac{\partial^2\sigma}{\partial X^2} & 0 \\ 0 & \frac{\partial^2\sigma}{\partial Y^2} \end{bmatrix} \tag{8}$$

The principal quantities of each element are then calculated [Equation (9)],

$$\lambda_1 = \left|\frac{\partial^2\sigma}{\partial X^2}\right| \text{ and } \lambda_2 = \left|\frac{\partial^2\sigma}{\partial Y^2}\right| \tag{9}$$

These principal quantities are used to compute proper element sizes h_1 and h_2 in the two principal directions using the condition [34],

$$h_1^2\lambda_1 = h_2^2\lambda_2 = \text{constant} = h_{\min}^2\lambda_{\max} \tag{10}$$

where h_{min} is the specified minimum element size, and λ_{max} is the maximum principal quantity for the entire model.

Based on the condition shown in Equation (10), the element size is generated using the given minimum element size h_{min}. Specifying too small h_{min} may result an excessive number of elements. While specifying too large h_{min} may obtain an inadequate solution accuracy or excessive analysis and meshing cycles. These factors must be considered prior to generate a new mesh. The H method build an entirely new mesh with different nodal locations from the old mesh. Interpolation of the solution from the old mesh to the new mesh should be used to increase the analysis solution convergence.

2.4 *Photoelasticity technique*

The photoelasticity technique can determine the state of stresses and crack propagation on a transparent material under both the static and dynamic conditions [35]. The technique provides a function of the difference of the principle stresses (σ_1–σ_2) or the maximum shear stress τ_m and the isochromatic–fringe–pattern as,

$$\sigma_1 - \sigma_2 = 2\tau_m = \frac{Nf_\sigma}{t} \tag{11}$$

where f_σ is the stress–optical constant, N is the order of the isochromatic fringe, and t is the specimen thickness.

The maximum shear stress is related with the stress components in the form,

$$(2\tau_m)^2 = (\sigma_x - \sigma_y)^2 + 4\tau_{xy}^2 \tag{12}$$

Similarly, by substituting Equations (1)–(3) into Equation (12), the relationship between the maximum shear stress and the stress intensity factors is obtained [36],

$$(2\tau_m)^2 = \frac{1}{2\pi r}\left[(K_I\sin\theta + 2K_{II}\cos\theta)^2 + (K_{II}\sin\theta)^2\right] + \frac{2}{\sqrt{2\pi r}}\sin\frac{\theta}{2}\left[K_I\sin\theta(1+2\cos\theta)\right] + K_{II}(1+2\cos^2\theta+\cos\theta) \tag{13}$$

Similarly, by substituting Equation (11) into Equation (13), the stress intensity factor for the opening mode can be expressed in the form [Equation (14)],

$$K_I = \frac{Nf_\sigma}{t}\frac{\sqrt{2\pi\, r_m}}{\sin\theta_m}\left[1+\left(\frac{2}{3\tan\theta_m}\right)^2\right]^{-\frac{1}{2}}\left(1+\frac{2\tan\frac{3\theta_m}{2}}{3\tan\theta_m}\right) \tag{14}$$

where r_m is the distance from crack tip to the farthest point on a given isochromatic loop and θ_m is the inclination angle of the crack plane as shown in Figure 5.

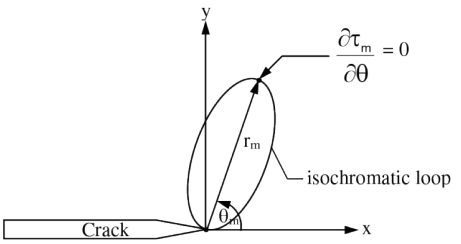

Figure 5: Distance r_m and angle θ_m of isochromatic loop.

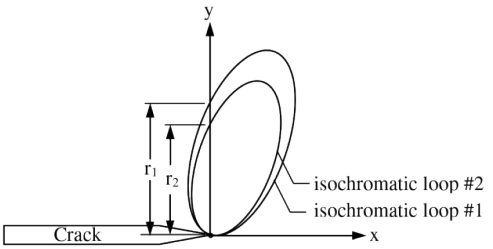

Figure 6: Distance rm of two isochromatic loops.

The position of the farthest point on a given isochromatic loop and the relationship between the stress intensity factors and the angle θ_m is obtained by minimizing Equation (13) with respect to θ ($\frac{\partial \tau_m}{\partial \theta} = 0$) to yield,

$$\left(\frac{K_{II}}{K_I}\right)^2 - \frac{4}{3}\left(\frac{K_{II}}{K_I}\right)\cot 2\theta_m - \frac{1}{3} = 0 \tag{15}$$

Equation (15) is used to determine the ratio of stress intensity factor (K_{II}/K_I) by measuring the angle θ_m at the point very closed to the crack tip. The stress intensity factor can be computed [35] by using the measured data from the two isochromatic loops along the line perpendicular to the crack plane ($\theta = 90°$) [36] as expressed in Figure 6 [Equation (16)].

$$K_I = \frac{f_\sigma}{t}\sqrt{2\pi r_1}\,\frac{(N_1 - N_2)}{1 - \sqrt{(r_1/r_2)}} \tag{16}$$

The photoelasticity prototype as depicted in Figure 7 is designed with the conceptual design as shown in Figure 1, built and used in this study. Photoelastic specimen was prepared and placed between polarizer and analyzer. Load condition is subjected on specimen and light source is on. Then isochromatic fringes can be investigated from the observer.

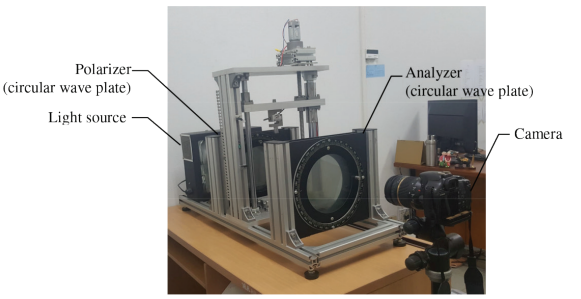

Figure 7: Photoelasticity Prototype.

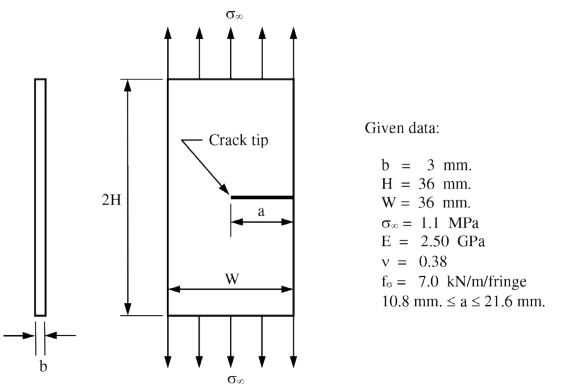

Figure 8: Problem statement of single edge cracked plate under tensile loading.

3 Applications

A single edge cracked plate under uniaxial tensile loading is used to evaluate the results of the adaptive remeshing technique and photoelasticity technique. The polycarbonate (PC) plates with dimensions of 36 × 72 × 3 mm are selected. Stress-optical constant of PC is 7.0 kN/m. Yellow monochromatic light with wavelength 589 nm is used. A neat plate and plate with hard inclusions are also studied.

A rectangular plate varied crack length per width (a/W) between 0.3 to 0.6 is used in the evaluation study. The plate is subjected to a far-field tensile stress of σ_∞ = 1.1 MPa along both the top and bottom edges as depicted in Figure 8. Because of symmetrical half model, the upper half of the plate is only used as a computational domain. Four analysis cases were performed with the crack length per width of 0.3, 0.4, 0.5, and 0.6. Figure 9 shows an example of the case of the crack length per width of 0.6. The adaptive remeshing model consists of six Q8-elements, six

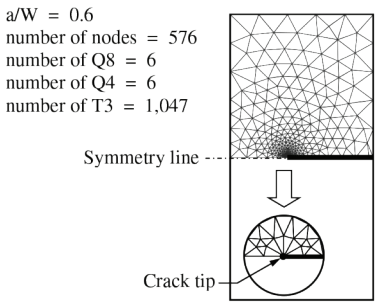

(a) Adaptive finite element model

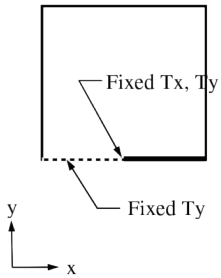

(b) Boundary conditions

Figure 9: Adaptive remeshing model of single edge cracked plate with a/W = 0.6.

Q4-elements and 1,047 of the T3 elements, with the total of 576 nodes.

The stress intensity factor for this problem is studied by Brown [24] following,

$$K_I = \sigma_\infty \sqrt{\pi a}\left[1.122 - 0.231\frac{a}{W} + 10.55\left(\frac{a}{W}\right)^2 - 21.71\left(\frac{a}{W}\right)^3 + 30.382\left(\frac{a}{W}\right)^4\right] \quad (17)$$

The computed stress intensity factor for the opening mode K_I obtained from the adaptive remeshing model is 1.22410 and the photoelastic technique is 1.22271, comparing to 1.22074 from Equation (17) with the differences of 0.28% and 0.16%, respectively.

Figure 10 shows the photoelastic result using the photo camera technique [37] for the neat plate of a/W = 0.6. The measured distance ri for each fringe N_i, i = 1 to 4, for the top and bottom fringe images are used to determine the average stress intensity factors. In this example four analysis cases of crack length ratios

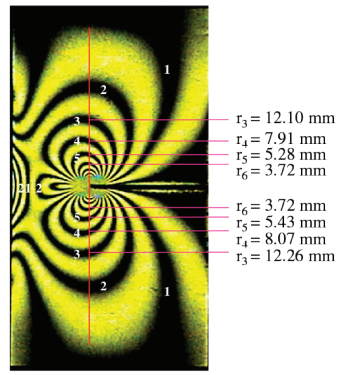

Figure 10: Photoelastic result of single edge cracked plate with a/W = 0.6.

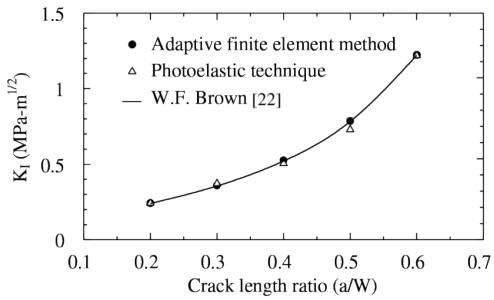

Figure 11: Comparative stress intensity factor K_I for single edge cracked plate.

of 0.3, 0.4, 0.5, and 0.6 are investigated. The stress intensity factor K_I results of the neat plate calculated from the finite element method and the photoelasticity technique are compared with those given by Brown for a/W = 0.3, 0.4, 0.5, and 0.6 as shown in Figure 11. The figure shows good agreement of the solutions for all cases of the crack length ratio. In these cases, the average K_I difference of adaptive remeshing model and photoelasticity technique is about 5.57%.

Then, crack-hard inclusion interaction is studied. An additional cracked plate configuration is investigated under varied crack length per width (a/W) between 0.2 to 0.599. Figure 12 shows the examples of cracked plate configurations at crack length per width (a/W) = 0.3 and 0.58. A hole or hard inclusion position is fixed. The hard inclusion is made of magnesium alloy AZ61. Constant E_{hard}/E_{plate} ratio, E_r = 28 is used. The stress intensity factor K_I obtained from both methods on the plates with a hard inclusion and comparing with one on a neat plate is shown in Figure 13. For all cases of the crack length ratio, the stress intensity factor K_I on

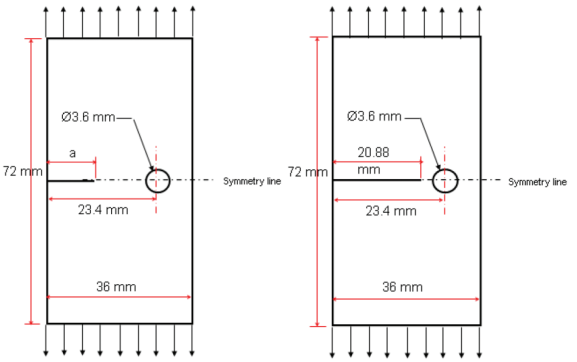

(a) a/W = 0.3 (b) a/W = 0.58

Figure 12: Position of a hole varied with crack length ratios on single edge cracked plate.

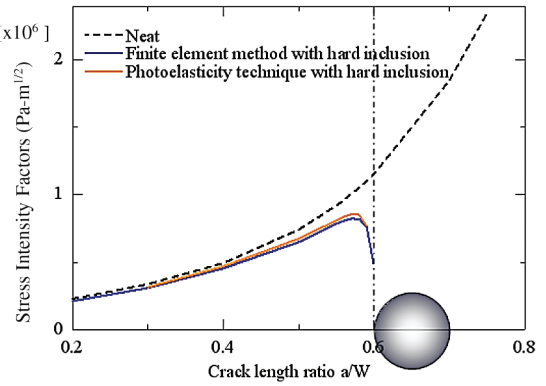

Figure 13: Stress intensity factor K_I varied with crack length ratios on single edge cracked plate.

a neat plate is higher than one on a plate with a hard inclusion. The K_I on a neat plate is increased if a/W is increased. The K_I difference between a neat plate and a plate with a hard inclusion is not significant if crack length per width (a/W) is small. The K_I on a plate with a hard inclusion is decreased when a/W is greater than 0.57. When crack propagates close to crack-hard inclusion interface, the stiffness of a hard inclusion or E ratio on interface is more significant than K_I and trend to stop crack propagation. This result implies that E ratio and crack length ratio affect to crack growth and crack-inclusion interaction, i.e. crack tip shielding. It shows good agreement of both solutions for all cases of the crack length ratio.

Furthermore, more varied E ratio, i.e. E ratio = 1.1, 1.2, 1.5, 2, 3, 4, 5, 10, 28, 50, and varied crack length per width (a/W) between 0.2 to 0.599 are studied.

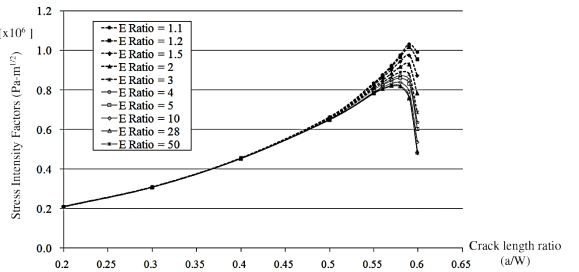

Figure 14: Stress intensity factor K_I varied with E ratio and crack length ratios on single edge cracked plate.

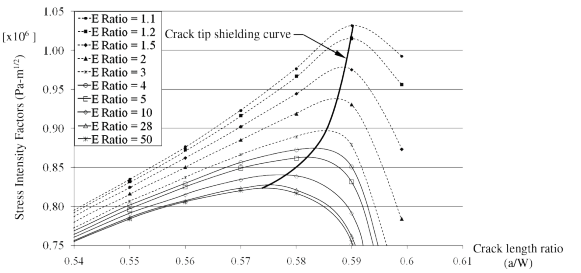

Figure 15: Crack tip shielding curves varied with E ratio and crack length ratios on single edge cracked plate.

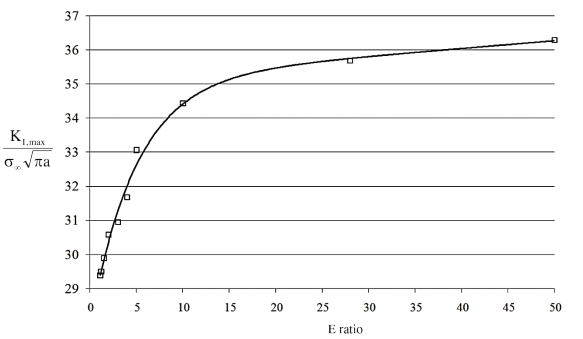

Figure 16: The normalized stress intensity factor $\frac{K_{I,\max}}{\sigma_\infty\sqrt{\pi a}}$ as a function of E ratio.

The adaptive remeshing technique is used to predict stress intensity factor K_I. Figure 14 represents the stress intensity factor K_I depending on E ratio and crack length ratio. If crack length per width is less than 0.4, E ratio is not affect to stress intensity factor K_I quantity. The crack length per width is significant to K_I when a/W is greater than 0.5. When E ratio increases, the maximum stress intensity factor K_I, max will decrease as shown in Figure 15. Figure 16 shows the normalized stress intensity factor $\frac{K_{I,\max}}{\sigma_\infty\sqrt{\pi a}}$ is a function of E ratio,

E_r. This function is convergence in exponential form [Equation (18)],

$$\frac{K_{I,\max}}{\sigma_\infty \sqrt{\pi a}} = 35.15e^{0.000625E_r} - 7.223e^{-0.2018E_r} \quad (18)$$

4 Conclusions

An adaptive remeshing technique using the eight-node quadrilateral element near the crack tip and photoelasticity method are presented to analyze two-dimensional fracture mechanics problems. The proposed methods are used to determine the stress intensity factors and crack-hard inclusion interaction for a single edge cracked plate under uniaxial tensile loading. The adaptive remeshing technique generates small elements in the crack region to increase solution accuracy. Larger elements are generated in the other regions where the small stress gradients to reduce number of elements and the computational time. The photoelastic technique is also employed to obtain the stress intensity factors. The photoelastic prototype is designed and built to use in this study. The benchmark problem of single edge cracked plate under tensile loading was used to evaluate the performance of the adaptive remeshing technique. Results of the stress intensity factors obtained from the adaptive remeshing method and photoelastic technique are compared. These results have demonstrated the applicability and advantages of the adaptive remeshing method for providing accurate prediction of the stress intensity factors. The single edge cracked plate with a hard inclusion is used in the study of crack-hard inclusion interaction or crack tip shielding. An additional cracked plate configuration, i.e. single edge cracked plate with a hard inclusion is investigated under varied crack length per width (a/W) between 0.2 to 0.599. The cracking tip shielding function of stress intensity ratio and E ratio is studied for varied E ratio between 1.1 to 50. The result shows that if E ratio increases, the maximum stress intensity factor K_I will decrease. The result shows that the normalized stress intensity factor is as a convergence exponential function of E ratio.

Acknowledgments

I extend my sincere thanks to all who contributed to preparing the instructions. Thammasat university, the Thailand Commission on Higher Education of Thailand (the National Research University Project), the National Science and Technology (NRCT), the Thailand Research Fund (TRF), Thammasat University, and the National Metal and Materials Technology Center (MTEC) who support this research.

References

[1] D. R. Jenkins, "Analysis of behavior near a cylindrical glass inclusion by scattered-light photoelasticity," *Experimental Mechanics*, vol. 8, no. 10, pp. 467–473, 1968.

[2] C. Atkinsons, "The interaction between a crack and an inclusion," *International Journal of Engineering Science*, vol. 10, no. 2, pp. 127–136, 1972.

[3] B. J. O. Toole and M. H. Santare, "Photoelastic investigation of crack-inclusion interaction," *Experimental Mechanics*, vol. 30, no. 3, pp. 253–257, 1990.

[4] S. A. Sushschenko, "Photoelastic analysis of stress concentrations in a two-dimensional model of hard inclusions in a metal matrix," *Tribology Transactions*, vol. 40, no. 2, pp. 386–390, 1997.

[5] E. E. Nugent, R. B. Calhoun, and A. Mortensen, "Experimental investigation of stress and strain fields in a ductile matrix surrounding an elastic inclusion," *Acta Materialia*, vol. 48, pp. 1451–1467, 2000.

[6] F. D. Corso, D. Bigoni, and M. Gei, "The stress concentration near a rigid line inclusion in a prestressed, elastic material. Part I. Full–field solution and asymptotics," *Journal of the Mechanics and Physics of Solids*, vol. 56, pp. 815–838, 2008.

[7] J. H. Kim and G. H. Paulino, "Simulation of crack propagation in functionally graded materials under mixed–mode and non–proportional loading," *International Journal of Mechanics and Materials in Design*, vol. 1, pp. 63–94, 2004.

[8] S. Phongthanapanich and P. Dechaumphai, "Adaptive delaunay triangulation with object-oriented programming for crack propagation analysis," *Finite Element in Analysis and Design*, vol. 40, no. 13–14, pp. 1753–1771, 2004.

[9] A. M. Alshoaibi, M. S. A. Hadi, and A. K. Ariffin, "An adaptive finite element procedure for crack

propagation analysis," *Journal of Zheijang Univeristy Science A*, vol. 8, no. 2, pp. 228–236, 2006.

[10] W. Limtrakarn and P. Dechaumphai, "Adaptive finite element method to determine K_I and K_{II} of crack plate with different $E_{INCLUSION}/E_{PLATE}$ ratio," *Transactions of the Canadian Society for Mechanical Engineering*, vol. 35, no. 3, pp. 355–368, 2011.

[11] B. N. Rao and S. Rahman, "An efficient meshless method for fracture analysis for cracks," *Computational Mechanics*, vol. 26, pp. 398–408, 2000.

[12] L. Luliang and Z. Pan, "Meshless method for 2D mixed–mode crack propagation based on voronoi cell," *ACTA Mechanica Solida Sinca*, vol. 16, no 3, pp. 231–239, 2003.

[13] Y. J. Chiuo, Y. M. Lee, and R. J. Tsay, "Mixed mode fracture propagation by manifold method," *International Journal of Fracture*, vol. 114, pp. 327–347, 2002.

[14] K. Xu, S. T. Lie, and Z. Cen, "Crack propagation analysis with galerkin boundary element method," *International Journal for Numerical and Analytical Methods in Geomechanics*, vol. 22, no. 5, pp. 421–435, 2004.

[15] R. Kitey, A. V. Phan, H. V. Tippur, and T. Kaplan, "Modeling of crack growth through particulate clusters in brittle matrix by symmetric–galerkin blundary element method," *International Journal of Fracture*, vol. 141, pp. 11–25, 2006.

[16] M. R. Ayatollahi and H. Safari, "Evaluation of crack tip constraint using photoelasticity," *International Journal of Pressure Vessels and Piping*, vol. 80, no. 9, pp. 665–670, 2003.

[17] S. W. Nam, Y. W. Chang, S. B. Lee, and N. J. Kim, "New Insights into plasticity-induced crack tip shielding via mathematical modelling and full field photoelasticity," *Key Engineering Materials*, vol. 345–346, pp. 199–204, 2007.

[18] P. C. Savalia and H. V. Tippur, "A study of crack-inclusion interactions and matrix-inclusion debonding using moire interferometry and finite elment method," *Experimental Mechanics*, vol. 47, no. 4, 2007.

[19] C. J. Christopher, M. N. James, K. F. Tee, and E. A. Patterson, "Evaluation of crack tip shielding using a photoelastic model," in *Proceeding the SEM XI International Congress on Experimental and Applied Mechanics*, pp. 371–380, 2008.

[20] C. J. Christophera, M. N. Jamesa, E. A. Patterson, and K. F. Teea, "A quantitative evaluation of fatigue crack shielding forces using photoelasticity," *Engineering Fracture Mechanics*, vol. 75, no. 14, pp. 4190–4199, 2008.

[21] M. N. James, Y. W. Lu, C. J. Christopher, and E. A. Patterson, "Full-field modelling of crack tip shielding via the 'Plastic Inclusion' concept," *Advanced Materials Research*, vol. 118–120, pp. 1–9, 2010.

[22] M. N. James, C. J. Christopher, Y. W. Lu, K. F. Tee, and E. A. Patterson, "Crack tip shielding from a 'Plastic Inclusion'," *Key Engineering Materials*, vol. 465, pp. 1–8, 2011.

[23] S. Bhat and S. Narayanan, "A computational model and experimental validation of shielding and amplifying effects at a crack tip near perpendicular strength-mismatched interfaces," *Acta Mechanica*, vol. 216, no. 1–4, pp. 259–279, 2011.

[24] T. Hiroshi, C. P. Paul, and R. I. George, *The Stress Analysis of Crack Handbook*. New York: ASME, 1985, pp. 46–54.

[25] T. L. Anderson, *Fracture Mechanics: Fundamentals and Applications*. Florida: CRC Press, 1994.

[26] W. Limtrakarn, "Stress analysis on crack tip using Q8 and adaptive meshes," *Thammasat International Journal of Science and Technology*, vol. 10, no. 1, pp. 19–24, 2005.

[27] O. C. Zienkiewicz and R. L. Taylor, *Finite Element Method*, 5th ed., Oxford, England: Butterworth–Heinemann, 2000.

[28] G. V. Guinea, J. Planas, and M. Elices "K_I evaluation by the displacement extrapolation technique," *Engineering Fracture Mechanics*, vol. 66, no. 3, pp. 243–255, 2000.

[29] R. Ramakrishnan, K. S. Bey, and E. A. Thornton, "Adaptive quadrilateral and triangular finite-element scheme for compressible flows," *AIAA Journal*, vol. 28, no. 1, pp. 51–59, 1990.

[30] P. Dechaumphai and E. A. Thornton, "Improved Finite Element Methodology for Integrated Thermal-Structure Analysis," NASA, Washington, DC, NASA CR 3635, Nov.1982.

[31] R. Lohner, K. Morgan, and O. C. Zienkiewicz, "Adaptive grid refinement for the Euler and

compressible Navier-Stokes equations," in *Proceedings the International Conference on Accuracy Estimates and Adaptive Refinements in Finite Element Computations*, 1984, vol. 2, pp. 189–202.

[32] P. Dechaumphai, "Adaptive finite element technique for heat transfer problems," *Journal of Energy Heat and Mass Transfer*, vol. 17, no. 2, pp. 87–94, 1995.

[33] J. Peraire, M. Vahjdati, K. Morgan, and O. C. Zienkiewicz, "Adaptive remeshing for compressible flow computation," *Journal of Computational Physics*, vol. 72, pp. 449–466, 1987.

[34] J. T. Oden and G. F. Carey, *Finite Elements: Mathematical Aspects*. New Jersey: Prentice-Hall, 1981.

[35] G. R. Irwin, "Discussion of the dynamic stress distribution surrounding a running crack – A photoelastic analysis," in *Proceedings of the Society for Experimental Stress Analysis*, 1958, vol. 16, no. 1, pp. 93–96.

[36] S. A. Paipetis and G. S. Holister, *Photoelasticity in Engineering Practice.* Netherlands: Elsevier Applied Science Publishers, pp. 181–204, 1985.

[37] M. A. Schroedl and C. W. Smith, *Local Stress near Deep Surface Flaws under Cylindrical Bending Fields*, Pennsylvania: ASTM International, pp. 45–63, 1973.